New Method for Determining Azimuths of ELF Signals Associated with the Global Thunderstorm Activity and the Hunga Tonga Volcano Eruption

Jerzy Kubisz[1], M. Gołkowski[2], Janusz Młynarczyk[3], Michal Ostrowski[4], and Adam Michalec[5]

[1]Astronomical Observatory, Jagiellonian University
[2]University of Colorado Denver
[3]AGH University of Science and Technology
[4]Jagiellonian University
[5]Jagiellonian University Astronomical Observatory

March 22, 2025

New Method for Determining Azimuths of ELF Signals Associated with the Global Thunderstorm Activity and the Hunga Tonga Volcano Eruption

J. Kubisz[1], M. Gołkowski[2], J. Mlynarczyk[3], M. Ostrowski[1†], A. Michalec[1†]

[1] Astronomical Observatory, Jagiellonian University, Kraków, Poland.

[2] Department of Electrical Engineering, University of Colorado Denver, Denver, USA.

[3] Institute of Electronics, AGH University of Science and Technology, Kraków, Poland.

Corresponding author: Michał Ostrowski (michal.ostrowski@uj.edu.pl)

† Emeritus.

Key Points:

- A new method for deriving wave arrival azimuths with parametric temporal filtering of electromagnetic waves in the ELF band is introduced.
- A multitude of thunderstorms on Earth varying during the day at different azimuths are resolved.
- The Hunga Tonga volcano eruption signals are diffracted by ≈10° when propagating in the Earth-ionosphere cavity over the polar regions.

Abstract

A new method is proposed for deriving Extremely Low Frequency (ELF) wave arrival azimuths using the wide range of signal amplitudes, contrary to previously applied high amplitude impulses only. The method is applied to observations from our new magnetic sensor in the Hylaty station with an18 bit dynamic range and a 3 kHz sampling frequency. We analyzed a day of January 15th, 2022, to test the procedure against the ability to extract ELF signals generated during the Hunga Tonga volcano eruption. With complementary filtering of power line 50 Hz signatures, precise azimuth information can be extracted for waves from a multitude of thunderstorms on Earth varying during the day at different azimuths. A phenomenon of successive regular variation - decay or activation - of thunderstorms activity with varying azimuth is observed, possibly due to passing over the solar (day/night) terminator, and signatures of azimuth direction change during this passage can be noted. We also show that the erupting Hunga Tonga volcano associated impulses dispersed due to a long propagation path are clearly revealed in the azimuth distribution with analysis using parameters fitted to measure slowly varying signals, but not for fast varying impulses. We show that the Hunga Tonga related signals arrive from the azimuth ≈10° smaller than the geographic great circle path. The

discrepancy is believed to be due to propagation through the polar region and in the vicinity of the solar terminator.

1. Introduction

Electromagnetic fluctuations in the extremely low frequency (ELF) band, defined here as 0.03 – 1000 Hz, provide a unique source of geophysical information that has not been exploited in depth (*Nickolaenko*, 1997; *Price*, 2016; *Nickolaenko et al.,* 2002). Naturally occurring ELF waves include Schumann resonances and ELF transients created by lightning, with often associated optical phenomena of sprites and elves. These waves are transmitted in the Earth-ionosphere waveguide and therefore provide a diagnostic on the lower ionosphere, which itself responds to solar changes and space weather phenomena (*Gołkowski et al.,* 2018). Ground based ELF observations have also become important support in identification of gravitational waves (*Coughlin et al.*, 2018).

Determining the arrival direction of natural emissions in the ELF/VLF bands has been of longstanding interest and is possible from a single receiver station if two or more components of the propagating fields are observed (*Kemp*, 1971; *Jones and Kemp*, 1970; *Kemp and Jones,* 1971). In the VLF band, the multimodal aspect of propagation in the Earth-ionosphere waveguide can yield polarization error in direction finding, which means signals are often analyzed in the frequency domain and efforts are made to quantify the polarization (*Gołkowski and Inan*, 2008; *Hosseini et al.,* 2018). In lightning detection networks such as the Vaisala GLD360 system, azimuth of VLF transients is determined in the time domain and polarization errors are mitigated by using only the first 200 μsec of the lightning signal (*Said et al.,* 2010).

In the ELF band the propagation is unimodal and typically two orthogonal measurements of the horizontal magnetic field are employed to find the arrival angle (*Nieckarz et al.,* 2011; *Füllekrug and Constable*, 2000). Nevertheless, there can be errors in the emission source direction finding at ELF claimed to be due to anisotropy of the ionosphere (*Füllekrug and Sukhorukov*, 1999) and scattering from the sharp conductivity boundaries such as ocean/land boundaries and the solar (day/night) terminator (*Mlynarczyk et al.,* 2017; *Nickolaenko et al.* 2018, 2021; *Schvets et al.* 2022). The impact of the ionospheric anisotropy on the signal propagation was discussed by *Nickolaenko and Sentman* (2007) to be observed as characteristic variations of signal ellipticity with the frequency. Techniques has been developed which seek to use two components of horizontal magnetic field and a vertical electric field to improve accuracy (*Jones and Kemp,* 1970; *Kemp and Jones,* 1971). In all cases of direction finding, operating over a larger bandwidth is known to reduce error (*Strangeways and Rycroft*, 1980; *Mlynarczyk et al.,* 2017; *Wood and Inan*, 2002, 2004).

As described in more detail below, the novelty of the present approach is the use of a difference technique that intrinsically introduces selective temporal filtering that can be used to remove power line interference or target specific temporal signatures. Thus a significant amount of the measurement data can be applied for the azimuth determinations, contrary to previous studies focusing on large ELF impulses in the data (see, e.g., a recent description in Nickolaenko et al. 2023) For

illustration of the possibilities of the proposed novel approach, we analyze observations from the day of January 15th, 2022, when occurrence of the Hunga Tonga (HT) volcano eruption created a strong compact ELF source (*Nickolaenko et al.,* 2022; Mezentsev *et al., 2022; Bor et al.,* 2023; see also Nickolaenko et al., 2023). We also present the capabilities of single site monitoring of global thunderstorm activity. In particular, at the figures one can note daily variations of the global thunderstorm activity, influenced by the Asian center at the azimuths ~90°, operating in the hours 6 - 10 h UT, shifting to the more powerful African center at the azimuths ~180° (12 - 18 h UT), and shifting toward the South American center at the azimuths ~-90° (18 - 22 h UT). The derived azimuths can be compared in detail with the list of selected reference azimuths from the Hylaty station presented in the Table 1. When inspecting the figures below one should not forget that the presented azimuth structures are significantly "filtered" by the parameters' sets selected in the applied azimuth derivation and the procedure provides more or less symmetric distribution for the source azimuth + or -180° .

Table 1. A list of selected reference geographic azimuths A, their respective anti-azimuths (indicated with an asterisk) and distances from the Hylaty ELF station.

Place	**A** [°] **(0°< A< 180°)**	**A** [°] **(-180°<A<0°)**	**Distance** [Mm]
Hawaii, Honolulu	0.4	-179.6 *	12.2
Angola, Lubango	9.6 *	-170.4	7.2
Nigeria, Lagos	27.5 *	-152.5	5.1
Hunga Tonga	32.9	-147.1 *	16.4
Alps, Graz	38.4 *	-111.6	0.6
Japan, Honshu	48.4	-131.6 *	8.6
Russia, Moscow	48.7	-131.3 *	1.3
Guinea Bissau	52.8 *	-127.2	5.4
Brazil, Belem	57.6 *	-122.4	7.4
Uruguay, Montevideo	58.4 *	-121.6	12.1
Brazil, Recife	59.3 *	-120.7	8.4
Papua New Guinea, Port Moresby	68.7	-111.3 *	13.3
Hong Kong	73.8	-106.2 *	8.3
Philippines, Manila	74.1	-105.9 *	9.4
Alps, Chamonix	78.6 *	-101.4	1.2
Vietnam, Hanoi	80.6	-99.4 *	7.8
Portugal, Porto	81.6 *	-98.4	2.6
Brazil, Manaus (Amazon region)	82.3 *	-97.7	9.7
Borneo	88.9	-91.1 *	10.1
Bangladesh, Dhaka	89.8	-90.2 *	6.4
Indonesia, Jakarta	98.3	-81.7 *	10.1
Haiti, Port-au-Prince	102.8 *	-77.2	8.8
India, Mumbai	108.4	-71.6 *	5.6
Pakistan, Karachi	108.7	-71.3 *	4.7
US, Florida, Orlando	118.9 *	-61.1	8.6

Nicaragua, Managua	121.2 *	-67.9	10.3
US, Georgia, Atlanta	124.5 *	-55.5	8.3
Madagascar	155.1	-24.9 *	8.0
Kenya, Mombasa	159.0	-21.0 *	6.1
DR Kongo, Kisangani	176.4	-3.6 *	5.4

2. ELA11 magnetic sensor

We use data (a data copy available at DATA_HYLATY_ELA11_2022_01_15, 2022) from our novel magnetic sensor ELA11 (Mlynarczyk et al., in preparation) with two perpendicular, NS and EW, active antennas installed at the Hylaty station (49.2° N, 22.5° E). The new sensor has a high 18-bit ADC resolution, enabling a much higher dynamic range than our ELA10 sensors deployed in the WERA system (Kulak et al., 2014; https://www.oa.uj.edu.pl/WERA). It also features a sampling frequency of 3 kHz (3004.81 Hz precisely), which is over three times higher than that of the ELA10 sensor. The increased dynamic range and higher bandwidth, as well as use of a Bessel anti-aliasing filter, enable improved resolution of individual impulses in the registered signal and better characterization of the temporal signal shape, as illustrated in Figure 1. The measured signal is provided by natural numbers in the ELA11 sensor units, with 1 pT magnetic field change equivalent to 12.68 sensor units. When analyzing the measured signal variations, one should keep in mind that the presented data have a zero reference point near the middle of the measurement range and only presented magnetic field variations have physical meaning.

The data analyzed in the present paper are available from an on-line repository (Kubisz 2023).

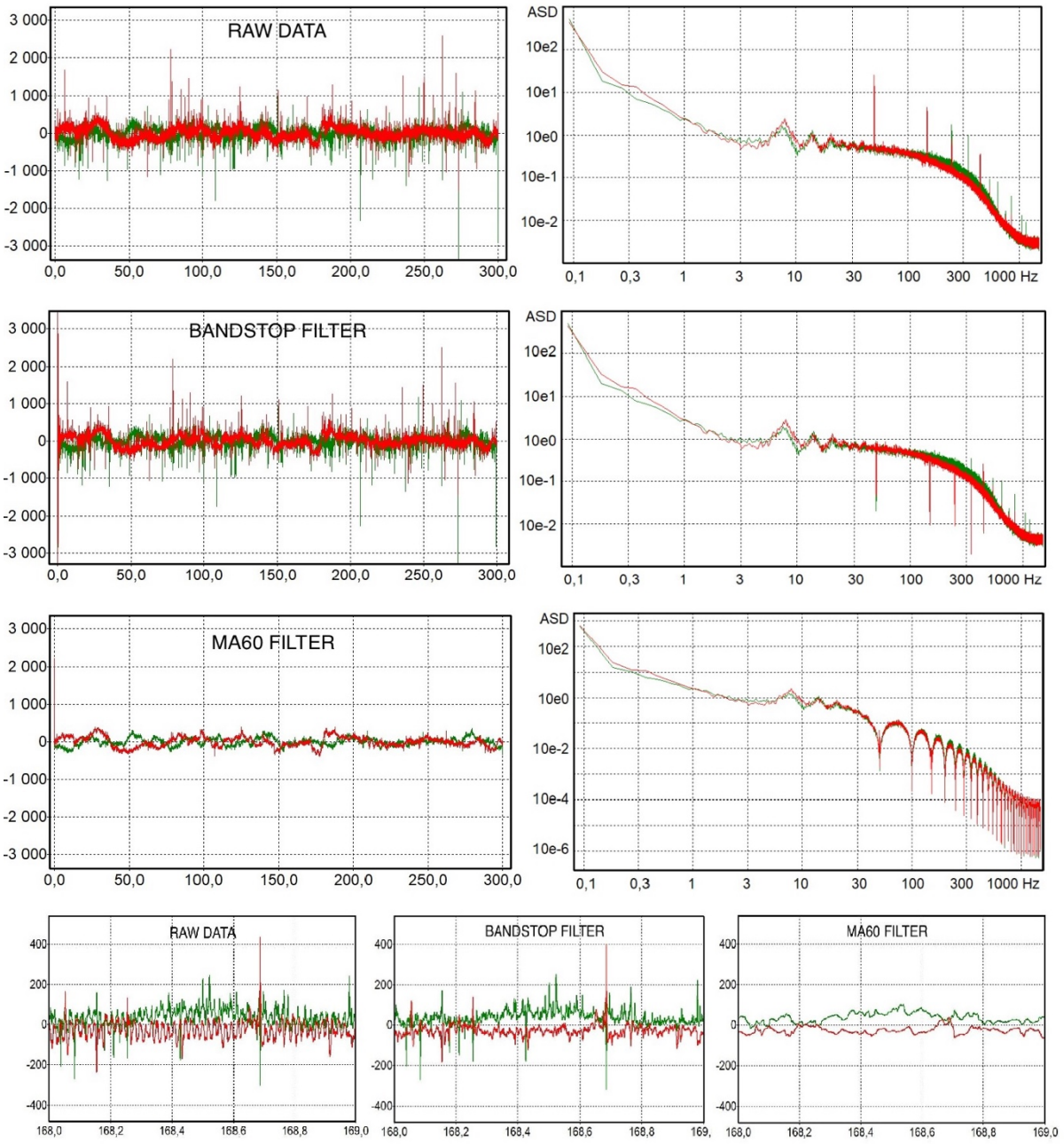

Figure 1. **A** (two panels at the top): An example 300 s (5 minutes') data stream in the receiver units and the associated log-log Amplitude Spectrum Density [pT / SQRT(Hz)] in NS (red) and EW (green) antennas from January 15th, 2022, 0:00-0:05 UT, from the ELA11 magnetometer at the Hylaty station; the same data and respective spectra are presented after electric power line filtering (see Sect. 3) with the bandstop filter (**B,** second row) and with the MA60 filter (**C,** third row); **D (**bottom**):** Detailed data comparison for a short 1 s range of unfiltered data (left panel) and filtered data with both the bandstop filter (middle panel) and the MA60 filter (right panel). Please, note different vertical scales at the presented spectra.

3. Derivation of ELF signal azimuths

Let us consider a geographic azimuth A measured from the North toward the East direction and we assume that the studied ELF waves have magnetic field component parallel to the Earth surface. We derive the signal azimuth of arrival, $A_{i,}$ using the registered signal changes in our NS and EW antennas between time instants t_i and t_{i+n} from the expression:

$$tan\ (A_{(i,\,n)}) = -\ \Delta B_{NS(i,\,n)} / \Delta B_{EW(i,\,n)} \qquad (1)$$

were $\Delta B_{(i,\,n)} = B_{(i+n)} - B_{(i)}$ is a difference between two signal measurements from a given magnetic antenna, NS or EW. Let us stress that the sign "minus" in the above expression is required due to our use of the measured ΔB_{EW}, not ΔB_{WE}. As pointed out above, the parameter n provides the time delay between successive signal samples applied for the azimuth derivation. For example, n=1 corresponds to two successive samples in the 3 kHz measurements, n= 60 corresponds to a delay of 0.02 s, the 50Hz electric power line period, and n=3000 to a delay of 1 second. Depending on positive or negative values of the derived $\Delta B_{(i,\,n)}$ we obtain the azimuths in the range (-180°, +180°). One should stress that for a single impulse the proposed approach – applying signal changes between two selected measurements instead of the full impulse amplitude – results in two azimuth values, A and A±180°, derived respectively for its growing part and declining part. Below, we apply this procedure to all successive measurements within the analyzed time range, applying the selected time delay n at each "i".

In the applied digital electronics, the measurement values are given by natural numbers, and with the applied 3 kHz sampling frequency, the derived differences between successive samples ΔB are often represented by small natural numbers or even zero. Such small values in the numerator or denominator of the right-hand side of Eq. (1) can drive the inverse tangent function to significant maxima of derived azimuth distributions at (±) 0, 90° and 180° degrees, as well as several discrete values 90°*(j/k), where j and k are small natural numbers. Additionally, the electric power grid associated signal at 50 Hz (see Figure 1) can introduce large scatter in the derived azimuth distribution and its possible arrangement respective to local electric power lines. Thus, when selecting signals for the azimuth derivation, we limit their magnitudes to pre-defined values for any given n by selecting the minimum and maximum limits r_{min} and r_{max} for the signal change parameter r = SQRT(ΔB_{EW}^2+ΔB_{NS}^2). Depending on the selected minimum and maximum values of this parameter one can study azimuth values for different wave (impulse) amplitudes, using the full available data above the level of electric power line signal variations, but not restricted to large individual magnetic peaks only. One should remember that the proposed procedure generates azimuth values differing by 180° between the rising and falling parts of the individual impulse. The analogous azimuth changes

would be obtained for positive and negative discharges as well as for signals propagating directly from the discharge location to the measuring station and the one reaching the station after propagation by the longer path around the Earth. Thus, in the presented figures we use an azimuth scale from -180° to +180° to present data resulting from Eq. 1, with expected symmetric A and A±180° values generated in this range by any single lightning generated impulse within the measurement range $r_{min} < r < r_{max}$. An inspection of the derived azimuth distributions in the figures below reveals a clearly visible difference between positive and negative azimuth distributions pointing to the existence of numerous temporally asymmetric signals with some superimposed background fluctuations and possible deviations of the impulse path from the geographic great circle.

The raw unfiltered data has a strong signature of the local electric power line at 50 Hz, which makes azimuth determination more difficult for small impulses. Specifically, from a visual inspection of the raw data (see Fig. 1D) we find that r values below r_{50Hz} ~100 (or ~8 pT in physical units) are not usable for the azimuth derivation when processing our raw data. To get around this limitation, we propose two optional approaches to extract azimuth information from the low amplitude signal fluctuations:

— by selecting the electric grid frequency n=60 (or its multiples) in Eq. 1 one removes significant part of the electric power line perturbations in the analysis (cf. Mitchell 1976) by using measurements in the same phase of this perturbing signal. However, the existing irregularities in the electric network signal shapes (see Figure 1D) still leave a noticeable scatter in the derived azimuths, and of course we lose the freedom to use different values of n in the analysis. Below, we positively tested the validity of such an approach (called also an *inter-period subtraction*) by comparing the azimuth distributions derived with small $r_{max} < r_{50Hz}$ with the ones for the larger impulses above the electric grid fluctuations.

— by filtering the 50 Hz component and its harmonics from the data one removes a significant part of its contribution to the analyzed signal. The situation is more complicated however, because the power line signal is subject to various fluctuations and any filtering procedure also perturbs the background ELF noise to be analyzed. Thus, it is essential to carefully evaluate possible 50 Hz filtering impact on the derived azimuths, which may significantly vary depending on the filtering method and the n, r_{min} and r_{max} parameters selected in the analysis. Below we will discuss application of two significantly different filtering procedures.

The first approach uses a third-order bandstop Butterworth filter (henceforth: “the bandstop filter”) which enables removal of the 50 Hz line fluctuations and its harmonic frequencies if they have significant amplitudes. A great advantage of a software filter over a hardware filter is that its center frequency and bandwidth can be adjusted to the processed signal, to minimize the distortions (see, e.g. Mlynarczyk et al. 2017). For studying short data samples (like the 5-minute or shorter time samples considered in our measurements) or individual strong impulses we typically use a filter with a

bandwidth of only 0.3 Hz at 50 Hz and 150 Hz (the precise central frequency is measured for each date file). Since the filter bandwidth is very narrow, it has little influence on the amplitude of lightning associated impulses. If 250 Hz and higher harmonic frequencies have a significant amplitude, one can filter them as well, but it is rarely necessary. The filter bandwidth at these higher harmonic frequencies is a little larger (we increment it by 0.2 Hz at each consecutive harmonic frequency). A slightly less intricate application of this filter is applied below where we analyze long 24h measurements, with present significant variations of the 50 Hz line: its intensity and central frequency, as well as the line width and more extended low intensity wings. For such cases we decided to use a uniform in all measurements, wider filter bandwidth of 1 Hz at the 50 Hz line as well as at its all registered harmonic frequencies. Thus, small observed variations of the line central frequency do not influence the filtering, but we note that the 50 Hz line wings as measured at our site sometimes extend off the applied 1 Hz exclusion bandwidth. Therefore, the remaining signal from the wings can still be left in the data after filtering, possibly perturbing low amplitude wave measurements. The raw ELA11 data are compared with the filtered data resulting from application of the above-described filter in Figure 1B and D.

A significantly different, second filtering procedure uses the moving average (MA60) filter, perhaps one of the most widely used FIR filters, here with averaging over the electric grid period of 0.02 s (i.e. over 60 successive measurement points). The filter fully removes the 50 Hz line and all its higher harmonic frequencies up to the considered here upper limit of 1500 Hz. In this case the procedure provides a low band pass filtering, significantly damping high frequency impulses, but preserving relatively undisturbed the low frequency ELF fluctuations. To see the effect, our raw data are compared below with the filtered ones in Figure 1C and D, showing that besides the 50 Hz periodic signal the filtering procedure removes (or significantly damps) all naturally occurring strong spikes.

Thus, when applying any of these 50 Hz filtering procedures, or not applying filtering at all, one should be careful in interpretation of the azimuths derived from the respective data for any set of the analysis parameters r_{min}, r_{max} and n. When possible, e.g., from a nearby/strong thunderstorms, one can compare the derived signal azimuth distributions with the one derived from the large impulses at $r > r_{50Hz}$. Also, the azimuth continuity of the signal from a single thunderstorm center, with its expected varying daily intensity and scatter, confirm reality and characterize accuracy of the measured azimuths. The studies, without considering powerful sources of ELF electromagnetic waves with known location (like the volcano eruption) or impulses from individual discharges registered in the VLF networks (e.g., WWLN or Vaisala) are not suitable to directly extract information about eventual systematic wave diffraction and respective azimuth modification along the signal path in the Earth-ionosphere cavity. However, such extended detailed analysis, involving studies of EM impulses from

227 individual lightning discharges registered by the WWLLN VLF network, lays outside the scope of the
228 present paper, with exception of the signal azimuth verification for the Hunga Tonga volcano eruption.
229 One should note that the applied filtering procedures introduce unphysical perturbed signal in
230 the very beginning of each filtered 300s data stream. Therefore, in this work we simply removed the
231 initial 2.6s of the data where such artifacts are observed from all analyzed filtered data samples.
232 Another option that one can use is to append the last part of the previous data file to the data range for
233 filtering and removing it afterwards.
234
235 **4. Azimuths of ELF electromagnetic waves registered in the Hylaty station**
236
237 To illustrate the range of possibilities of the proposed ELF signal azimuth analysis applied to the
238 ELA11 receiver measurements we selected the day of January 15th, 2022 (0-24 h UT). We processed
239 the data to extract information on natural ELF wave fields anisotropies and additionally, to check
240 constraints on revealing the ELF signature associated with the HT volcano eruption (*Nickolaenko et*
241 *al.,* 2022; *Bor et al.,* 2023). The eruption signatures in the time range 4:15-5:50 UT for the main
242 eruption and in the time range 8:35-9:30 UT for the next weaker one, are visible in our data, as
243 presented in the 24-hour dynamic spectrum evolution at Figure 2. The discussed below azimuth
244 distributions provide an additional tool to extract the HT electromagnetic signal from a background
245 thunderstorms' noise superimposed in the plot.
246 Before inspecting the daily evolution of spectrum and azimuth let us explain that to reveal
247 variations in all considered frequency and amplitude ranges we performed fine tuning of the presented
248 values to the plot color scale by using two numerical factors, the first was multiplying the data while
249 the second was subtracted from the data. Thus, in Figure 2 one can analyze nearly all spectra in the full
250 range of 1-165 Hz, clearly revealing also the secondary HT eruption signatures, on the expense that
251 strong HT signal is presented as white, being unresolved above the applied color scale.
252

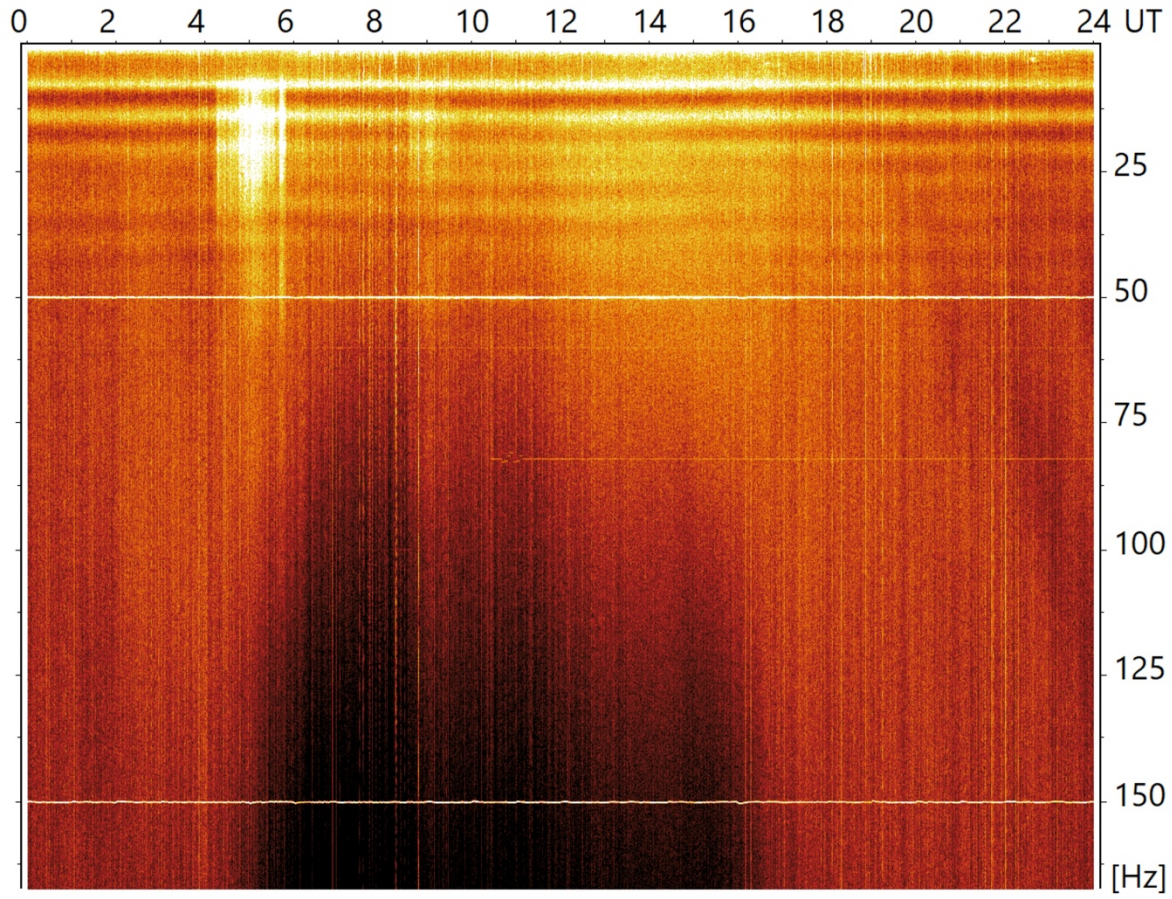

Figure 2. Evolution of the ELF signal power spectrum in the EW antenna on January 15th, 2022, from 0 till 24 UT. Each vertical line shows a successive 75-second spectrum in the frequency range up to 165 Hz. We used the Hann window in computations to minimize nearby thunderstorms' noise in the plot. The HT eruption signatures are clearly visible for frequencies less than 50 Hz at 4:15-5:50 UT and a somewhat weaker eruption from 8:35 till 9:30 UT.

In Figure 2 one can note continuous horizontal stripes of at least seven Schumann resonances, a 50 Hz power line, and its harmonic at 150 Hz, also a weak 60 Hz line and the 82 Hz (possibly a Russian submarine communication) line switching on at 10 UT. One can also notice a decrease in power of higher frequency components in the spectra (steepening of the spectrum) from approximately 5 till 16 UT (darker colors at higher frequencies). Strong succession of impulsive signals generated during the HT main eruption occurs during the HT primary eruption and again but slightly less pronounced during the secondary. The analogous, but less pronounced HT related features are also visible in the (not presented) power spectrum evolution plot for the NS antenna, as expected for the HT azimuth (see below).

Now, let us analyze a daily (Jan. 15th, 2022) evolution of ELF signal azimuths derived as explained above in Section 3. One should remember that differences of the considered source distances lead to modification of intensity and dispersion of individual impulses. Below, we

273 demonstrate how selection of parameters n, r_{min} and r_{max} enables one to extract azimuths for particular
274 ELF signals and thunderstorm regions. In the plots, we originally searched for signatures of the HT
275 eruption near its geographic azimuth $A_{HT} = 32.8°$ and A_{HT}-180° = -147.2° to learn that it is significantly
276 shifted to ≈20° and -160°, respectively. The distance to the erupting volcano is significant, $D = 16400$
277 km, so we expected and confirmed in the measurements below that the volcano originated signals are
278 subject to significant dispersion even for the direct path propagation.
279

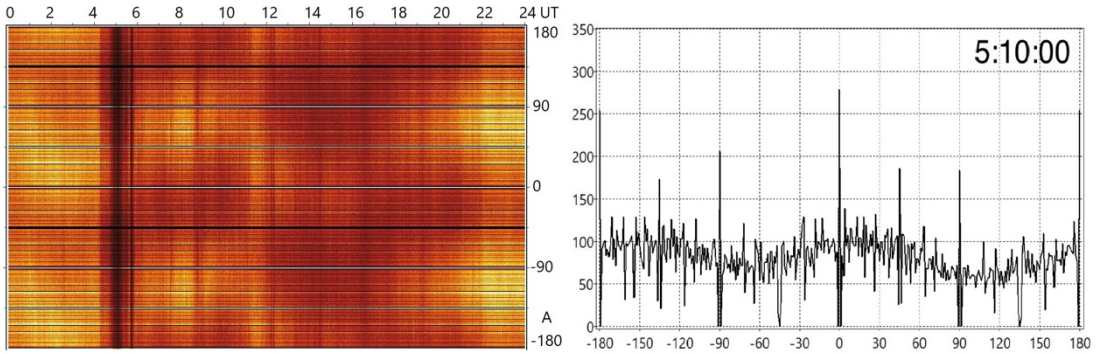
0 2 4 6 8 10 12 14 16 18 20 22 24 UT
180
90
0
-90
A
-180
5:10:00
-180 -150 -120 -90 -60 -30 0 30 60 90 120 150 180

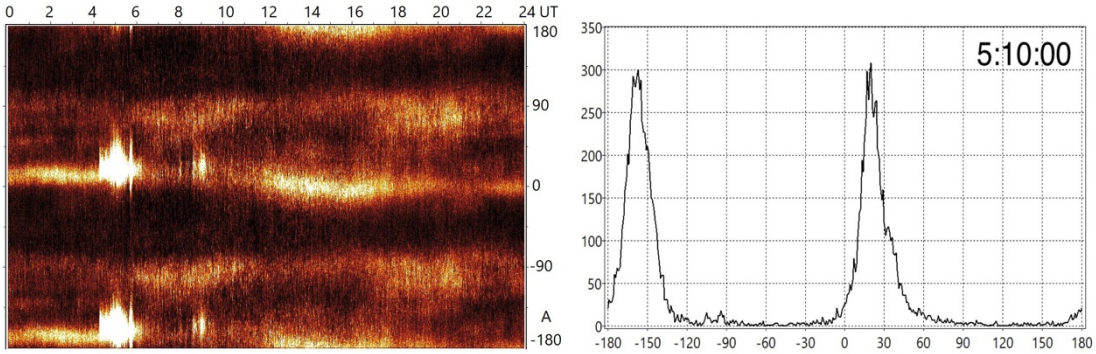
0 2 4 6 8 10 12 14 16 18 20 22 24 UT
180
90
0
-90
A
-180
5:10:00
-180 -150 -120 -90 -60 -30 0 30 60 90 120 150 180

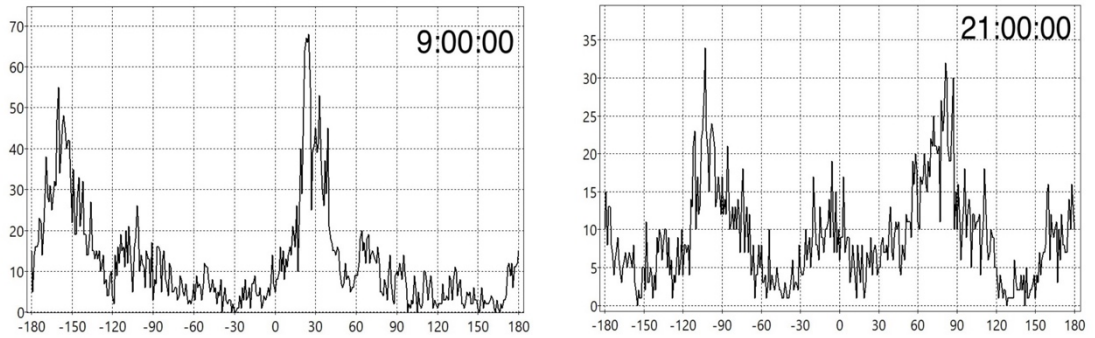
9:00:00
-180 -150 -120 -90 -60 -30 0 30 60 90 120 150 180
21:00:00
-180 -150 -120 -90 -60 -30 0 30 60 90 120 150 180

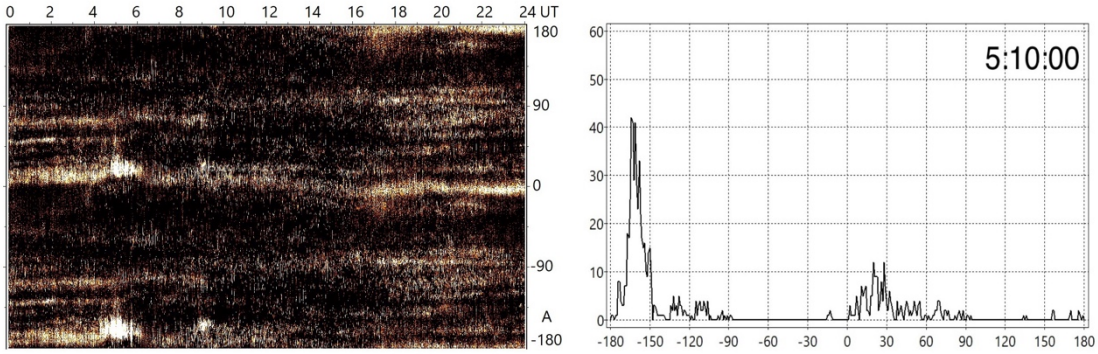
0 2 4 6 8 10 12 14 16 18 20 22 24 UT
180
90
0
-90
A
-180
5:10:00
-180 -150 -120 -90 -60 -30 0 30 60 90 120 150 180

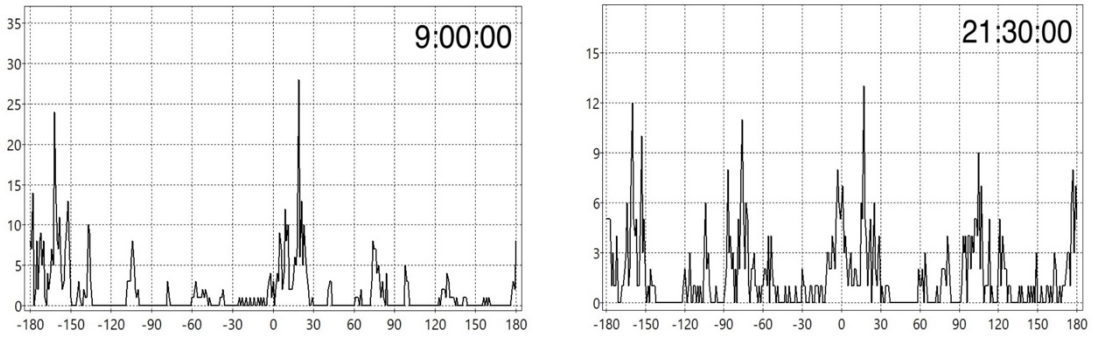
9:00:00
-180 -150 -120 -90 -60 -30 0 30 60 90 120 150 180
21:30:00
-180 -150 -120 -90 -60 -30 0 30 60 90 120 150 180

280

Figure 3. Azimuth daily evolution and distributions of derived azimuths during 75 s time bins beginning in selected times, derived with the raw data for n=60. We present plots for **A** (two panels at the top) (r_{min}=10, r_{max}=30) and 5:10:00 UT; **B** (4 panels in rows 2 and 3) (r_{min}=200, r_{max}=300) and 5:10:00 UT, 9:00:00 UT and 21:00:00 UT; and **C** (4 panels at the bottom, rows 4 and 5) (r_{min}=500, r_{max}=5000) and 5:10:00 UT, 9:00:00 UT and 21:30 UT. At vertical axes of the azimuth distributions, we present the number of measurements per one-degree azimuth range. Note vertical scale changes between the presented azimuth distribution plots.

Let us start with the raw unfiltered data. Here to subtract the 50 Hz line contribution from the data we either select n=60 (Δt_{50Hz} = 0.02 s) to compare ELF signal changes in the same phase of the electric power line signal or we select only high amplitude ($r > r_{50Hz}$) impulses/waves for any selected n. When analyzing the results in the first considered case for n=60 we see that preferential values of r are comparable or above the electric line fluctuations, as the tests with $r_{max} < r_{50Hz}$ show a significant random smoothing of the azimuth distribution as seen in Figure 3A. In a period of the high intensity HT eruption most of r measurements for n=60 are above r_{max} selected for this plot and thus excluded from the plot, leading to a vertical dip in the azimuth distribution measurement (cf. Mezentsev et al., 2022). On the other hand, a clear HT signal dominating the azimuth distribution during the eruption (4:15 – 5:50 UT and near 9:00 UT) is visible in Figure 3B, where results for r a few times larger than r_{50Hz} (still with n=60) are presented. Outside of the eruption times, the thunderstorm activity produces in this analysis quite diffuse, not well resolved structures. To reach high directional resolution of the incoming waves one must select $r_{min} \gg r_{50Hz}$, as presented in Figure 2C. Then, both the HT primary and secondary eruption signatures are clearly visible, but also several separate azimuth ranges of thunderstorm activity, varying during the day, can be clearly resolved outside the HT eruption periods. In conclusion, use of n=60 to subtract the electric grid background seems to be fully effective only for large amplitude signals, while irregularities of the electric grid signal presented in Figure 1D (left plot) introduce significant scatter in azimuths derivations for smaller r.

From inspection of Figures 3B and C one should note, however, that the mean measured HT signal azimuth from our Hylaty ELF station appears to be near 20°, which is more than 10 degrees smaller than the HT geographic azimuth, A_{HT} = 32.8°. An azimuthal deviation of similar magnitude from the true geographic azimuth for ELF measurements was also noted by Füllekrug and Sukhorukov (1999) to occur when the waves propagated near the high conductivity of the Pacific Ocean. Mlynarczyk et al. (2017) found that azimuthal deviations can be caused by diffraction from the solar terminator nonuniformity. Following those past studies, we interpret the presently measured difference as resulting from the signal deflection at ionospheric nonuniformities in the northern and southern polar regions as well as at the solar terminator. In this context it is worthy to note that the terminator

was passing over the Hylaty station in time of the volcano main eruption and the HT signal direct path to the station was close to the terminator in the polar region. In principle, also a contribution from the powerful African thunderstorm center at A<20° could contribute to this distribution shift, but we note a fortunate significant calming of this signal (see Figure 4 and Figure 5 below) in the beginning of the HT eruptive activity what makes such an explanation doubtful.

One can also minimize the influence of electric grid signal at the derived azimuth distribution at any other selected n by considering values of r much higher than the ones in the grid signal. One should note here that a change of the grid signal from its minimum to maximum occurs at a time scale of ¼ $\Delta t_{50\mathrm{Hz}}$ (or n=15) and thus effective grid signal variations for n<15 may be significantly smaller that the full amplitude $r_{50\mathrm{Hz}}$. Thus, let us consider the case with n=3 (a time step of 1 ms) and the required large signal changes with r_{min}=300. At the resulting azimuth distribution presented on Figure 4 one can note quite efficient azimuth resolution in the plot. However, we also note that the HT signal signature completely disappears from the plot. In fact, such an effect is expected for signals from a distant source since the impulses diminish their amplitudes and experience significant dispersion during propagation, contributing to the ELF signal with smaller r, outside the parameter range selected for this derivation. Removal of the HT contribution from the azimuth distribution reveals interesting structures on the remaining plot. In the analyzed winter day, a significant ~12h range of low thunderstorm activity appears on the plot, between ca. 5 UT and 16:30 UT for thunderstorm centers close to azimuths 0° and ±180°, while regularly shifting with time for growing azimuths, with the quiescence range roughly 6 UT–18 UT at 45° but extending only up to ~14 UT at the azimuth stripe visible above 90°. Following earlier publications we interpret this regular structure in the studied winter day at the Northern hemisphere as switching-off of the thunderstorm activity at successive azimuths by the propagating solar terminator. A similar but somewhat less regular process of azimuth dependent switching-on of the thunderstorm activity appears in the evening (see also Figure 5 below). Let us also note that careful inspection (also in the studies of filtered data below) of the considered thunderstorm switching-off ranges suggest existence of small upturns to higher azimuths before the quiescence phase (cf. Shvets et al. 2022). If real, such behavior could indicate the effect of the signal diffraction at the terminator passing over the given thunderstorm site. One more important feature is present in these azimuth data with absent HT signatures. An active thunderstorm center with the measured azimuth close to A_{HT}=32.8° (and -147.2°) initiated its activity before the HT main eruption (Figure 4B) and was continuing activity during the main eruption phase, as we observed in the respective azimuth distributions before and during the main eruption. Thus, it is important to know that this signal from the HT geographic azimuth is not the volcano eruption signature, but a superimposed thunderstorm activity.

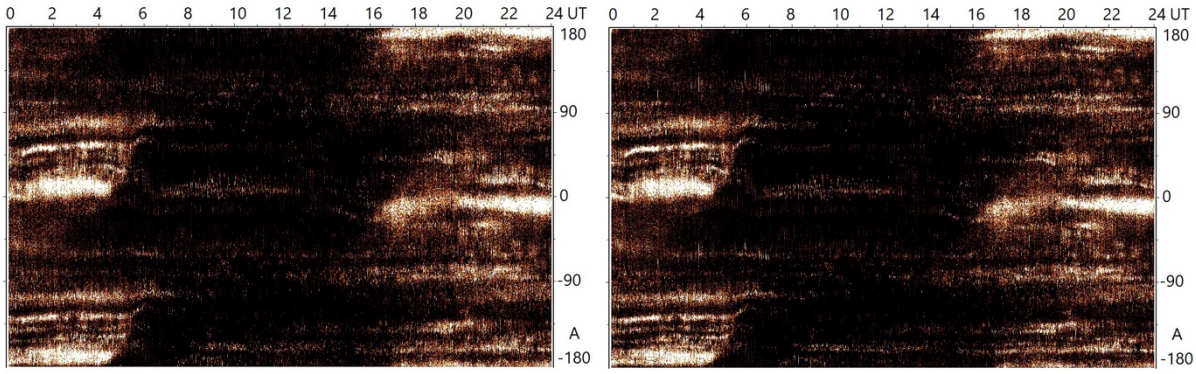

Figure 4. Comparing daily ELF signal azimuth distributions derived with n=3, r_{min}=300 and r_{max}=3000 for **A**. the raw data (left); and **B**. the data with 50 Hz line filtered using the bandstop filter (right). Existing slight differences between the plots are hardly visible.

Now, let us consider another suggested option for removing effects of 50 Hz line fluctuations from the analysis by removing the power line periodic signal and its harmonics with filtering procedures discussed in Section 3. Let us start with applying the bandstop filter. The resulting daily varying distribution of signal azimuths derived from such filtered data is presented in Figure 4B, where we selected for presentation quickly varying high amplitude impulses analyzed with r_{min}=300 and n=3. In this case the filtering procedure allows for tiny but visible improving azimuth resolution as compared to the unfiltered data in Figure 4A. In effect we reveal and can track during the day numerous thunderstorm centers at different azimuths with slightly improved resolution. One should note that, as mentioned above, some thunderstorm activity appears also close to the HT geographic azimuth of ≈33° long before the volcano first eruption and the accompanied signal is continuously observed also during the HT main eruption, which is not visible in this plot with small n and $r_{min} >> r_{50Hz}$ Thus, we interpret here the respective maximum ≈33° in the azimuths' distribution during the eruption as the projected local thunderstorm activity, not related to the HT. On the other hand, by selecting r_{min} and r_{max} below the value of r_{50Hz} one can clearly reveal the signal with azimuths from the HT first and second eruptions, but with a large scatter. It shows that the applied filtering procedure cleans nicely the individual high amplitude impulses but is not able to do the same for the low amplitude fluctuations in the data. At this figure (Fig. 4) one may note the previously discussed azimuth dependent switching-off of the thunderstorm activity in the morning, finishing in a few cases with the azimuth distributions' upturns.

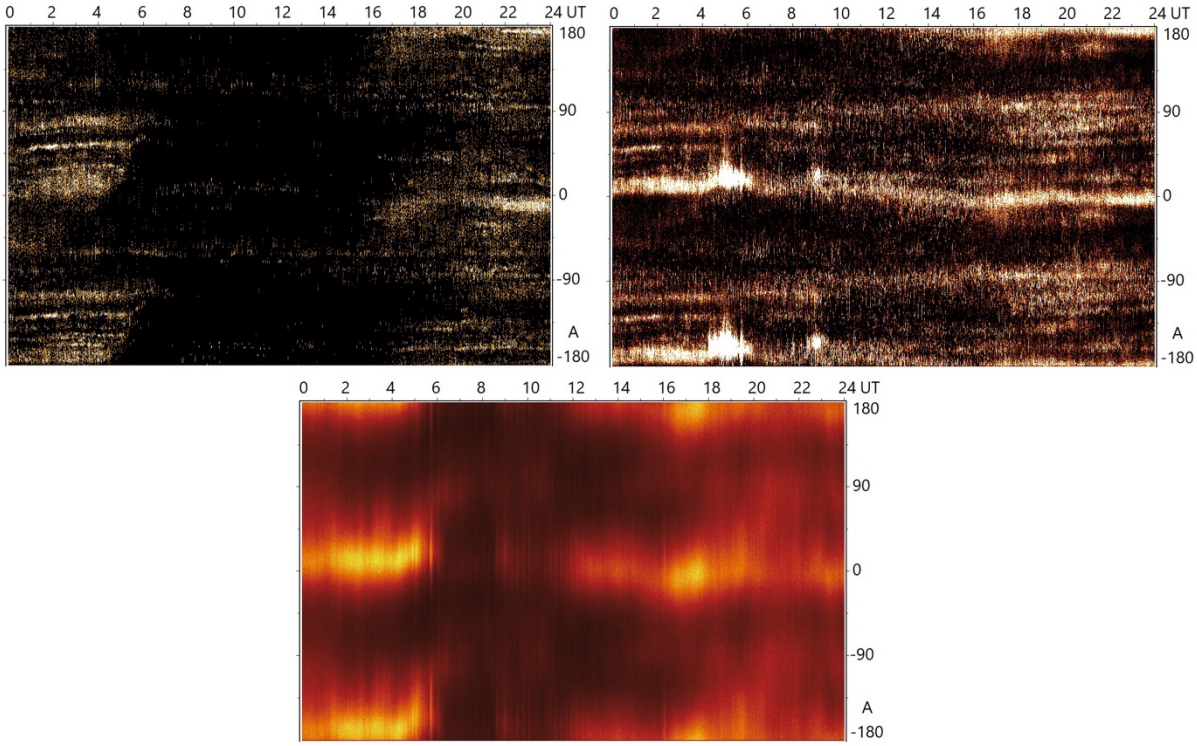

Figure 5. Comparing daily ELF signal azimuth distributions derived with n=1 for the data with filtered 50 Hz line using **A**. the bandstop filter for r_{min}=300 and r_{max}=3000 (upper left); **B**. the MA60 filter for r_{min}=6 and r_{max}=30 (upper right) and **C**. the bandstop filter for r_{min}=6 and r_{max}=30 (bottom).

A quite different output is obtained when using the MA60 filter. In effect, as presented on Figure 1C, D, the impulses with steep rising and declining slopes are removed or at least highly attenuated in the filtered data. Thus, only the slowly varying or low amplitude signals are available for the analysis with a selected n below 60. Let us perform azimuth analysis in such data with $r_{max} < r_{50Hz}$. Example distributions resulting for n=1, r_{min}=6 and r_{max} = 30 are compared in Figure 5 with the results for the data cleaned using the bandstop filter. It is important to note that the characteristic azimuth stripes from thunderstorms visible in this figure for the MA60 filter (Figure 5B) coincide with the azimuths derived from high amplitude impulses using the bandstop filter (Figure 4B and 5A) as well as the ones without any filtering for $r_{min} >> r_{50Hz}$ (Figure 4A). Thus, somehow to our surprise the MA60 filtered data presented in Figure 1D preserved the azimuth information in the slowly varying signal, including clear signatures from the HT eruption at A≈20°. It is contrary to slowly varying signals in the bandstop filtered data providing highly dispersed azimuth distributions in Figure 5C. One should note that the HT azimuth distribution derived in this analysis matches well to the ones derived from both the bandstop filtered data and, from the raw data, when using large amplitude signals with larger n. This fact confirmed consistency of all considered approaches and in the same time reality of the obtained azimuths.

Another interesting case in this analysis can be studying ultra-low frequency magnetospheric PC fluctuations (see e.g. Kivelson, M.G. and Russell, C.T. 1995), studied earlier in the Hylaty station by Nieckarz (2016) and Nieckarz & Michałek (2020). To illustrate this possibility, we selected a large n=3000 and -- from the data inspection -- we choose $r_{min}=10^3$ and $r_{max}=10^4$ for the analysis to obtain results presented in Figure 6. It is interesting to note that the registered long wave azimuths are well constraint to some discrete directions, forming a regular time pattern and revealing clear differences in the observed trends between waves propagating in the early and late hours of the day, and in the daytime. We note that on Jan. 15th, 2022, there is lack of such high amplitude waves in time periods of 5-7 UT and 17-18:30 UT, close to the sunrise and the sunset in the Hylaty station (where the local time = UT + 1h in winter). The measurements of large amplitude short spikes create more diffuse "background" stripes of colored points at the plot, around azimuths of nearby thunderstorms.

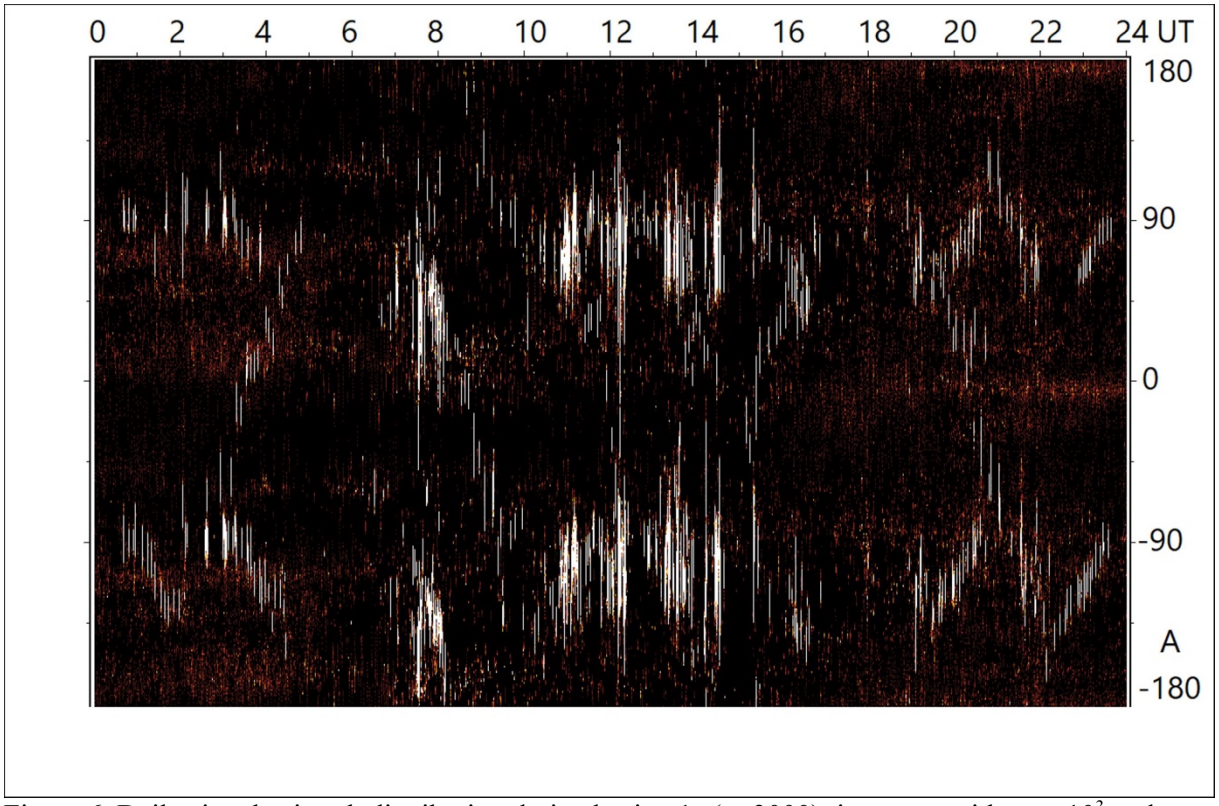

Figure 6. Daily signal azimuth distribution derived using 1s (n=3000) time step, with $r_{min}=10^3$ and $r_{max}=10^4$ for the non-filtered data. White lines result from long (~1 s or longer) high amplitude waves, while red/yellow points in the background are created by short large lightning spikes in the data.

5. Conclusions

In the present study we show that with high quality ELF measurements, like our data from the ELA11 sensor, one can separate ELF signals emitted from numerous thunderstorm regions distributed along the Earth. This very fact indicates that in many time instants signals from individual thunderstorm

regions dominate the measurements. It is contrary to our original expectation that in the majority of observations – with the exception of large impulses - one would register a superposition of signals from sources from a wide range of azimuths

To analyze azimuths of the registered ELF signals we proposed a new simple, but powerful method comparing signal changes in two perpendicular magnetic antennas, as presented in Section 3. By selecting 3 parameters in this method, the maximum and minimum signal changes, r_{max} and r_{min}, and the time scale for these changes characterized with n, one can study waves/impulses with different frequencies and amplitudes, to take into account the modification (dispersion) of the signal shape during its propagation in the earth-ionosphere cavity. Thus, by selecting different sets of (r_{max}, r_{min}, n) one can study different aspects of the thunderstorms' distribution and its varying activity. The derived azimuths are more precise after one remove interference from the electric grid.

In the case of analyzing the signal changes smaller or comparable to the ones from the 50 Hz electric power line perturbations, significant scatter is observed in the derived azimuth distribution. A possibility to take into account such periodic perturbations is to measure the natural ELF signal changes in the same phase of the electric power line signal, by selecting n=60 in our data for the respective time delay between measurements. However, as one could see in Figure 1D, the power line signal registered in our Hylaty station is not as regular as we would wish to have and accuracy improvement of azimuth resolution for small measured amplitudes r appears to be quite moderate. On the other hand, the analysis resolves separate thunderstorm directions for large impulses. Overall, usage of n=60 falls short of the main intended goal of enabling study of azimuth information of small amplitude ELF impulses.

To deal with this problem we tested the filtering of the 50 Hz signal from the data with two significantly different filtering procedures. The bandstop filtering appears excellent in "cleaning" steep impulses/spikes in the ELF signal and providing a significant improvement for derived azimuths. The procedure decreases dispersion of azimuths derived for high amplitude impulses and it enables reasonable thunderstorm direction resolution using even smaller spikes. Unfortunately, the small amplitude waves in such filtered signal do not show clear azimuth separation, possibly due to remaining perturbations left from the wide and thus not fully removed wings of the 50 Hz line.

When inspecting Figure 1D, at first glance the results of the applied low pass MA60 filter does not give much hope for extracting detailed directional information about numerous thunderstorms. However, despite the removal/deformation of the quickly varying impulses, this signal still contains quite precise information about waves propagating from many different azimuths, also when analyzing low amplitude signal changes with $r \ll r_{50Hz}$. Apparently, short impulses in both antennas are corrected in the same proportion, without a noticeable change of the azimuth values resulting from equation 1. Studying of such low amplitude or slowly varying signals is essential in identifying emissions from distant sources, with impulses smoothed due to large dispersions.

A fortunate (for ELF research!) strong and extended in time point-like electromagnetic emission from the HT eruption allowed us to analyze the propagation of ELF waves along a trajectory crossing the Earth polar region and to test our azimuth derivation method for extracting a particular source signal from the general electromagnetic activity in the earth-ionosphere cavity. The long >16 Mm direct propagation path introduces significant dispersion into the volcano lightnings' generated spikes. In effect, the HT azimuth signal is clearly visible when limiting analysis to the slowly varying signals, while analysis of high amplitude and fast changing impulses does not show any clear HT signature. Moreover, in this last case one can monitor in the azimuth distribution evolution map the thunderstorm signals from directions close to the HT geographic azimuth, which are overshadowed in the lower amplitude measurements by a dominating HT contribution. The analysis also shows the research potential of azimuths distribution studies, by allowing a robust identification of the weaker secondary HT eruption. The method allows for precise measurement of the significant (>10°) HT ELF signal azimuth deviation from the geographic azimuth due to wave deflection in the polar region and/or the waves propagation near the solar terminator, in the process discussed earlier by Mlynarczyk et al. (2017).

Acknowledgements

Authors are grateful to Astronomical Observatory of the Jagiellonian University for continues support of ELF research and operation of the WERA magnetic sensors' array. The development of ELA11 sensor has been supported by the National Science Centre, Poland, under Grant 2015/19/B/ST10/01055. This research was partly funded by the National Science Centre, Poland, grant 2023/49/B/ST9/02777. Mark Golkowski was supported by National Science Foundation Award AGS 2312282 to University of Colorado Denver. The authors are grateful to Alexander Nickolaenko and two anonymous referees for critical remarks and valuable advice helping to improve the manuscript.

Open research

The data analyzed in the present paper are available from an on-line repository (Kubisz 2023).

References

Bor, J., Bozoki, T., Satori, G., Williams, E., Behnke, et al. 2023. Responses of the AC/DC global electric circuit to volcanic electrical activity in the Hunga Tonga-Hunga Ha'apai eruption on 15 January 2022. *Journal of Geophysical Research: Atmospheres*, **128**, e2022JD038238. https://doi.org/10.1029/2022JD038238

Coughlin, M. W., Cirone, A., Meyers, P., Atsuta, S., Boschi, et al. 2018. Measurement and subtraction of Schumann resonances at gravitational-wave interferometers. *Physical Review D*, ***97***(10), 102007. https://doi.org/10.1103/PhysRevD.97.102007

Füllekrug, M., Sukhorukov, A. I. 1999. The contribution of anisotropic conductivity in the ionosphere to lightning flash bearing deviations in the ELF/ULF range. *Geophysical Research Letters*, ***26***(8), 1109-1112. https://doi.org/10.1029/1999GL900174

Füllekrug, M., Constable, S. 2000. Global triangulation of intense lightning discharges. *Geophysical Research Letters*, **27**(3), 333-336. https://doi.org/10.1029/1999GL003684

Gołkowski, M., Inan, U. S. 2008. Multistation observations of ELF/VLF whistler mode chorus, Journal of Geophysical Research, **113**, A08210, doi:10.1029/2007JA012977.

Gołkowski, M., Sarker, S. R., Renick, C., Moore, R. C., Cohen, et al. 2018. Ionospheric D region remote sensing using ELF sferic group velocity. *Geophysical Research Letters*, **45**(23), 12-739. https://doi.org/10.1029/2018GL080108

Hosseini, P., Gołkowski, M., Chorsi, H. T., Gedney, S. D., Moore, R. C. 2018. Using eccentricity to locate ionospheric exit points of magnetospheric whistler mode waves. *IEEE Transactions on Geoscience and Remote Sensing*, **56**(12), 7049-7061**.** doi: 10.1109/TGRS.2018.2847605

Jones, D. L., & Kemp, D. T. (1971). The nature and average magnitude of the sources of transient excitation of Schumann resonances. Journal of Atmospheric and Terrestrial Physics, 33(4), 557-566.

Kemp, D. T. (1971), The global location of large lightning discharges from single station observations of elf disturbances in the Earth-ionosphere cavity, *J. Atmos. Terr. Phys., 33*, 919–927, doi:10.1016/0021-9169(71)90091-2.

Kemp, D. T., and D. Llanwyn Jones (1971), A new technique for the analysis of transient ELF electromagnetic disturbances within the Earth-ionosphere cavity, *J. Atmos. Terr. Phys., 33,* 567–572.

Kivelson, M.G. and Russell, C.T. (1995). Introduction to Space Physics, *Cambridge University Press*, p. 330. ISBN 9780521457149.

Kubisz, J. 2023 [Dataset] A set of measurement data from the ELA11 magnetometer from January 15, 2022, Hylaty Station, Poland
https://uj.rodbuk.pl/dataset.xhtml?persistentId=doi:10.57903/UJ/NSRSLE

Kulak, A., Kubisz, J., Klucjasz, S., Michalec, A., Mlynarczyk, J., et al. 2014. Extremely low frequency electromagnetic field measurements at the Hylaty station and methodology of signal analysis. *Radio Science*, **49**, 361– 370. https://doi.org/10.1002/2014RS005400

Mezentsev, A., Nickolaenko, A. P., Shvets, A. V., Galuk, Yu. P., Schekotov, A. Yu., Hayakawa, M., Romero, R., Izutsu, J., Kudintseva, I. G. 2022. Observational and model impact of Tonga volcano eruption on Schumann resonance, Journal of Geophysical Research: Atmospheres, 128, e2022JD037841. https://doi.org/10.1029/2022JD037841

Mitchell, V. B. 1976. Schumann resonance−some properties of discrete events, *Journal of Atmospheric and Solar-Terrestrial Physics*, 38, 77−82

Mlynarczyk, J., Kulak, A., Salvador, J. 2017. The accuracy of radio direction finding in the extremely low frequency range. *Radio Science*, **52**(10), 1245-1252. https://doi.org/10.1002/2017RS006370

Nickolaenko, A. P. 1997. Modern aspects of Schumann resonance studies. *Journal of Atmospheric and Solar-Terrestrial Physics*, **59**(7), 805-816. https://doi.org/10.1016/S1364-6826(96)00059-4

551 Nickolaenko, A. P., Hayakawa, M. 2002. Resonances in the Earth-ionosphere cavity. Vol. **19**. *Springer*
552 *Science & Business Media*.
553
554 Nickolaenko, A. P., Galuk, Yu P. Hayakawa, M., 2018. Deviations of source bearing in the Earth–
555 inonosphere cavity with the day-night non-uniformity. *Telecommunications and Radio Engineering*,
556 **77**(11), 995-1016 DOI: 10.1615/TelecomRadEng.v77.i11.50
557
558 Nickolaenko, A. P., Galuk, Yu P. Hayakawa, M., Kudintseva, I. G. 2021. Model source
559 bearings of Q-bursts for observations in Antarctica, *Journal of Atmospheric and Solar-*
560 *Terrestrial Physics*, 222, 105723. https://doi.org/10.1016/j.jastp.2021.105723
561
562 Nickolaenko, A. P., Schekotov, A. Y., Hayakawa, M., Romero, R., Izutsu, J. 2022. Electromagnetic
563 manifestations of Tonga eruption in Schumann resonance band. *Journal of Atmospheric and Solar-*
564 *Terrestrial Physics*, **237**, 105897. https://doi.org/10.1016/j.jastp.2022.105897
565
566 Nickolaenko, A. P., Sentman, D. D. 2007, Line splitting in the Schumann resonance oscillations, Radio
567 Science, 42, RS2S13. https://doi:10.1029/2006RS003473
568
569 Nickolaenko, A. P., Shvets, A.V., Galuk, Yu.P., Schekotov, A. Y., Hayakawa, M., et al. 2023. Power
570 flux in the Schumann resonance band linked to the eruption of Tonga volcano on Jan. 15, 2022. (Two
571 point measurements of Umov-Poynting vector). *Journal of Atmospheric and Solar-Terrestrial Physics*,
572 **247**, 106078. https://doi.org/10.1016/j.jastp.2023.106078
573
574 Nieckarz, Z. (2016). Imprints of Natural Phenomena and Human Activity Observed During 10 Years
575 of ELF Magnetic Measurements at the Hylaty Geophysical Station in Poland, *Acta Geophysica* 64,
576 2591-2608. DOI: 10.1515/acgeo-2016-01
577
578 Nieckarz, Z., Kulak, A., Zieba, S., Odzimek, A. (2011), Cloud-to-ground lightning dipole moment
579 from simultaneous observations by ELF receiver and combined direction finding and time-of-arrival
580 lightning detection system, *Journal of Geophysical Research*, **116**, D08107.
581 doi:10.1029/2010JD014736.
582
583 Nieckarz, Z. and Michałek, G. (2020). Long-term observation of magnetic pulsations through the ELF
584 Hylaty station located in the Bieszczady Mountains (south–eastern Poland), *J. Space Weather Space*
585 *Clim.* 10, 59. https://doi.org/10.1051/swsc/2020063
586
587 Price, C. 2016. ELF electromagnetic waves from lightning: The Schumann resonances. *Atmosphere*,
588 **7**(9), 116. https://doi.org/10.3390/atmos7090116
589
590 Shvets, A.V., Nickolaenko, A.P., Koloskov, A.V., Yampolsky, Y.M., Budanov, et al. 2022. Day
591 after day variations of arrival angles and polarisation parameters of Q bursts recorded at
592 Antarctic station "Akademik Vernadsky", *Journal of Atmospheric and Solar-Terrestrial*
593 *Physics*, **229**, 10581. https://doi.org/10.1016/j.jastp.2021.105811
594
595 Strangeways, H. J., Rycroft, M.J. 1980, Systematic errors in VLF direction-finding of whistler ducts—
596 II, *Journal of Atmospheric and Solar-Terrestrial Physics*, **42**, 1009– 1023.
597 https://doi.org/10.1016/0021-9169(80)90114-2
598
599 Wood, T. G., Inan U. S. 2002. Long-range tracking of thunderstorms using sferic measurements,
600 *Journal of Geophysical Research*, **107**(D21), 4553, doi:10.1029/2001JD002008.
601

602 Wood, T. G., Inan U. S. 2004. Localization of individual lightning discharges via directional and
603 temporal triangulation of sferic measurements at two distant sites, Journal of Geophysical Research,
604 **109**, D21109, doi:10.1029/2004JD005204.
605